Journal: Palaeogeography, Palaeoclimatology, Palaeoecology

Title: Controls on the altitude of Scandinavian cirques: what do they tell us about palaeoclimate?

Rachel P. Oien[1] (rachel.oien1@abdn.ac.uk) Iestyn D. Barr[2] (I.Barr@mmu.ac.uk), Matteo Spagnolo[1] (m.spagnolo@abdn.ac.uk), Robert G. Bingham[3] (r.bingham@ed.ac.uk), Brice R. Rea[1] (b.rea@abdn.ac.uk), and John Jansen[4] (jdj@ig.cas.cz)

*corresponding author

[1] University of Aberdeen, School of Geosciences, Department of Geography & Environment, St. Mary's Building, Elphinstone Road, Aberdeen, United Kingdom AB24 3TU

[2] Manchester Metropolitan University, Department of Natural Sciences, Manchester, United Kingdom M1 5GD

[3]University of Edinburgh, School of GeoSciences, Drummond Street, Edinburgh, United Kingdom EH8 9XP

[4]GFU Institute of Geophysics, Czech Academy of Sciences, Prague, Czechia

Keywords: ELA, Cirques, Palaeoclimate, Climate, Glacier

ABSTRACT

Cirques are glacially eroded, bowl-shaped depressions, characterised by steep headwalls and flat or overdeepened floors. Given their association with past glaciers, cirques are sometimes used as proxies for palaeoclimate. However, cirques are shaped over multiple glacial cycles, and their usefulness as palaeoclimate indicators therefore remains open to question. In this paper, we map 3984 glacier-free cirques across the Scandinavian Peninsula and analyse variations in cirque floor altitude (CFA). We explore the relationships between CFAs and cirque aspect, latitude, longitude, and distance to the coast. We test the validity of using CFAs as indicators of palaeoclimate through comparison with the equilibrium-line altitudes (ELAs) of 513 modern cirque glaciers. Results indicate that both CFAs and modern cirque-glacier ELAs decrease with latitude and vary with aspect, being generally lowest on east-facing slopes. However, the clearest and strongest trend in both CFAs and modern cirque glacier ELAs is an increase in elevation with distance from the modern coast (i.e., distance 'inland'). This likely indicates that similar climatic gradients, particularly an inland reduction in precipitation, acted to regulate former sites of glacier initiation (reflected by CFAs) and modern glacier ELAs. This would imply that CFAs are a useful proxy for palaeoclimate. However, we note that both CFAs and modern ELAs reflect the general topography of this region (with increasing elevations moving inland), and the glacial history of the area (indirectly linked to palaeoclimate) may have played a role in regulating where cirques have formed. For these reasons, we suggest that palaeoclimatic interpretations derived from CFAs should be treated with caution.

1.0 Introduction

The equilibrium-line altitude (ELA) is the elevation on a glacier surface where net annual accumulation and ablation are equal. Therefore, the ELA is largely determined by regional climate (the dominant control on accumulation and ablation) (Nesje, 1992; Ohmura et al., 1992; Ipsen et al., 2017; Ohmura and Boettcher, 2018), though other local topoclimatic factors (e.g. topographic shading, snow and ice redistribution and aspect) also contribute (Olyphant, 1977; Morris, 1981; Torsnes et al., 1993; Coleman et al., 2009; Hughes, 2010; Křížek and Mida, 2013). Given this association, glacier ELAs are often used to infer spatial and temporal variations in climate and palaeoclimate (e.g. Sutherland, 1984; Caseldine and Stötter, 1993; Torsnes et al., 1993; Oien et al., 2020; Rea et al., 2020). Therefore, palaeo-ELAs are important as palaeoclimatic indicators because they are the result of changed precipitation and temperature, which control glacial surface mass balance over time and cirques are one way of obtaining palaeo-ELAs (e.g. Torsnes et al., 1993; Kern and László, 2010; Barr and Spagnolo, 2015a; Barr and Spagnolo, 2015b; Barr et al., 2017; Pearce et al., 2017; Ipsen et al., 2017; Wallick and Principato, 2020).

The most robust way to estimate palaeo-ELAs is to generate 3D reconstructions of former glaciers. However, a number of simpler methods are also used, particularly when considering ELAs across large and/or remote areas. One of the simplest ways is to map and measure cirque floor altitudes (CFAs) (e.g. Torsnes et al., 1993; Kern and László, 2010; Barr and Spagnolo, 2015a; Barr and Spagnolo, 2015b; Barr et al., 2017; Pearce et al., 2017; Ipsen et al., 2017; Wallick and Principato, 2020). The premise behind this approach is that cirques (bowl-shaped depressions, characterised by steep headwalls and flat or overdeepened floors sometimes occupied by small lakes; Evans and Cox, 1974; Vilborg, 1977; Fredin et al., 2013) are formed where glaciers develop and erode their underlying bedrock. When these glaciers are relatively small and largely confined to the cirque (e.g., at the onset and termination of glacial cycles), the CFA (i.e., the lowest point within a cirque) roughly approximates the glacier's ELA. Though this approach only provides an approximation of the ELAs of former cirque glaciers, it has been widely used to investigate regional patterns in palaeo-ELAs, and sometimes to make associated inferences about palaeoclimate (e.g. Evans, 1999; Benn and Lehmkuhl, 2000; Barr and Spagnolo, 2015b). Despite this widespread use, there are several caveats associated with using CFAs as indicators of former

cirque glacier ELAs. In particular, since cirque glaciers form at different times in different places, regional trends in CFA are unlikely to reflect palaeo-ELA trends at any single point in time. This raises questions about the usefulness of CFAs as proxies for palaeoclimate.

In this study, we map the distribution of glacier-free cirques in the Scandinavian Mountains and analyse variations in the associated CFAs. We compare these patterns with the ELAs of modern cirque glaciers in the region (Oien et al., 2020). The aim is to establish how palaeoclimatic information can most efficiently be extracted from cirque floor elevation distributions, despite their potentially time-transgressive origins, evolution and occupation (Rudberg, 1994; Evans, 1999; Barr and Spagnolo, 2013). The Scandinavian Mountains are well suited to this study, as they lie on a passive margin, have a comparatively well-constrained glacial history, and both cirques and extant cirque glaciers are widespread.

2.0 Study Area

2.1 Geology and Geography

The study area (Figure 1) extends ~2000 km N-S along the Scandinavian Mountains, and up to 400 km W-E from the Norwegian Sea inland into Sweden. Topographic elevations typically increase inland, extending up to ~1500 m in the north and ~2400 m in the south. The geology is mostly a result of the Caledonian orogeny, from 400-700 Ma (Holtedahl, 1920; Stephens, 1988; Lidmar-Bergström, et al., 2000), when collisions between orogenic belts and exotic terranes created a series of Precambrian and Palaeozoic crystalline metamorphic rocks (Etzelmüller et al., 2007). The closure of the Iapetus Ocean and collision with Laurentia caused crustal thickening, generating a stable crust that makes up the Fennoscandian Shield (Stephens, 1988). The majority of cirques in the south are located within areas classified as upland mountains with moderate slopes and alpine relief (Etzelmüller et al., 2007). This region is known for extensive plateaux steeply cut by glacial valleys (Etzelmüller et al., 2007). More recently, glacial isostatic adjustment due to the demise of the Fennoscandian ice sheet has resulted in an uplift of up to ~1 to 15 mm yr^{-1} across the Scandinavian Peninsula (Lambeck et al., 1998a; Lambeck et al., 1998b; Steffen and Kaufmann, 2005; Angus and Peltier, 2010).

2.2 Glaciation

Extensive glaciers and ice sheets have repeatedly occupied and shaped the Scandinavian landscape over multiple Quaternary (and pre-Quaternary) glacial cycles (e.g. Mangerud, 2008; Mangerud et al., 2011; Fredin et al., 2013; Olsen et al., 2013a; Olsen et al., 2013b; Hughes et al., 2016; Stroeven et al., 2016). These glaciations have generated a wide range of erosional and depositional features, resulting in a dramatic landscape of elongated overdeepened basins (often occupied by lakes), fjords, glacial valleys, and cirques. At present, thousands of glaciers occupy the Scandinavian Mountains, ranging in size from small cirque glaciers to extensive ice caps (Nesje, 2009; NVE, 2017)

2.3 Climate

Climatic patterns across the Scandinavian Peninsula are heavily influenced by the North Atlantic Oscillation (NAO) and Arctic Oscillation (AO) (Nesje, 2008). These systems regulate pressure gradients, which control temperature, precipitation, and storms. The interplay of these pressure systems sometimes results in comparatively warm (between 0 and 2˚C) wet (up to 2000 mm/year in the southern coastal region) winters, or cold (between 0 and -16˚C, particularly in the northern region) dry winters (Norwegian Meteorological Institute, 2021). In the southern Scandinavian Mountains, precipitation is also regulated by the Jet Stream, with a dominant wind direction from the S/SW, and can reach 6000 mm/year in coastal areas but decreases dramatically inland to 500-750 mm/year (Torsnes et al., 1993; Nesje et al., 2008; Nesje, 2009; Winsvold et al., 2014; Norwegian Meteorological Institute, 2021). Winter precipitation (Figure 1b) and summer temperatures (Figure 1a) are the main climatic controls on modern-glacier surface mass balance (Ohmura et al., 1992; NVE, 2017; Ohmura and Boettcher, 2018; Oien et al., 2020).

3.0 Methods

We mapped glacier-free cirques using a 10 x 10 m digital terrain model (DTM) with a vertical accuracy of ±1-6 m, overlain with 10 m contours from the Norwegian mapping authority (Kartverket; Hoydedata.no) (Figure 2). Most of the mapped cirques coincide with cirque locations identified by Rudberg (1994) and the definition of a cirque by Evans and Cox (1974) and Vilborg (1984). Once mapped, we divided cirques by latitude into southern <64°N and northern >64°N sub-populations (‘macro-regions’), following Oien et al. (2020). The division is roughly based on

climate, with the northern macro-region defined as 'polar/subpolar' due to its proximity to the polar front while the southern macro-region is 'temperate' due to the influence of the North Atlantic Current (Tveito et al., 2000; Oien et al., 2020).

Each cirque was mapped as a polygon (Figure 2): we extracted the CFA as the single lowest elevation DTM grid cell contained within the polygon (Figure 3a). To assess possible controls on CFA, several other attributes were derived: cirque aspect was calculated using the GIS tool ACME (Spagnolo et al., 2017) (i.e. aspect is defined as the mean azimuth (0-360°) determined from every pixel converted to radians and averaged within the cirque) (Evans, 1977; Evans, 2006b; Barr and Spagnolo, 2015a); cirque latitude and longitude were recorded using the centroid of each feature; and cirque distance from the modern coast, excluding fjords (Norwegian Sea, Figure 3) was calculated in ArcGIS (following Oien et al., 2020). In addition to mapping cirques, the ELAs of 513 modern cirque glaciers (Figure 3b) in the region were analysed, based on the dataset from Oien et al. (2020).

4.0 RESULTS

4.1 Cirque-floor altitudes (CFAs)

A total of 3984 glacier-free cirques were mapped throughout the Scandinavian Mountains: 2947 in the northern region, and 1037 in the southern region (Figure 3). For the population as a whole, CFAs range from 23 m to 2088 m (Table 1). In the northern region, the mean CFA (591 m) is notably lower than in the southern region (1195 m). Cirques in the northern region are also typically closer to the modern coastline (mean distance = 40.8 km) than those in the south (mean distance = 104.7 km) (Table 2).

4.2. CFA variations with latitude and longitude

For the population as a whole, CFAs show a statistically significant, $p<0.01$, decline to the north and east (Figure 4), although the linear regression between CFA and latitude is stronger (R^2 = 0.441) than between CFA and longitude (R^2 = 0.212). Despite these general trends, considerable variability is present between each (southern and northern) region. For example, in the northern region, CFAs decline with latitude (Figure 5; R^2 = 0.113, panel a), but more weakly than for the entire cirque population. In the southern region, CFAs rise then fall with latitude (Figure 6; R^2 =

191 0.114, panel a). Overall, it appears that the population-wide latitudinal trend in CFA is partly a
192 reflection of differences between the northern and southern regions (Figure 4a). In both the
193 northern and southern regions, CFAs show an eastward rise then fall with longitude (Figure 5b,
194 Figure 6b). The ELAs of modern cirque glaciers in the region show broadly similar latitudinal and
195 longitudinal trends to those highlighted for the CFA population (and sub-populations) but as
196 expected, lie a few hundred metres above (Figure 4a, 4b, 5a, 5b, 6a, 6b).
197
198 *4.3. CFA variations with aspect*
199 The mean vector aspect for the entire cirque population is 35.5°, which compares with 40.7° for
200 modern cirque glaciers. However, these values show some regional variation. In the northern
201 region, the cirque and modern cirque glacier vector means are 36.5° and 42.8°, respectively. In the
202 southern region, these values are 33.2° and 38.4°, respectively (Figure 7). However, overlapping
203 95% confidence intervals suggest that inter-regional differences in mean aspect (Figure 7) are
204 unlikely to be statistically significant. CFAs and modern cirque glacier ELAs show some
205 variability with aspect. For example, E-facing cirques typically have lower CFAs by ~150 m
206 (median = 642 m) than those facing S/SW (median = 828 m) (Figure 8), for the entire population.
207 Fourier (harmonic) regression (Evans and Cox, 2005; Evans, 2006a) indicates that these
208 relationships show no statistically significant overall trends, $p>0.05$ (Table 3). Aspect vector
209 strength for the entire cirque population is 29%, which compares to 69% for the modern cirque
210 glaciers. This difference likely stems from the entire cirque population reflecting conditions during
211 multiple periods of past glaciation, whereas the distribution and aspect of modern cirque glaciers
212 reflects conditions during a single 'snapshot' of marginal glaciation (i.e., the present) when
213 topoclimatic factors (e.g. shading) play a strong role in regulating glacier location. This is
214 consistent with the 'law of decreasing glacial asymmetry with increasing glacier cover' (Evans,
215 1977).
216
217 *4.4. CFA variations with distance to the coast*
218 The attribute most strongly related to CFA is the distance to the modern coastline, with the
219 population as a whole (7.7 m/km; $R^2 = 0.750$; RMSE = 211; Figure 4d) and northern (7.7 m/km;
220 $R^2 = 0.701$; RMSE = 182; Figure 5d) and southern (4.9 m/km; $R^2 = 0.465$; RMSE = 227; Figure
221 6d) sub-regions showing a statistically significant increase inland, $p<0.01$ (Table 3). This trend is

also seen in modern cirque glacier ELAs as a whole (5.8 m/km; $R^2 = 0.668$; RMSE = 177; Figure 4d) and within the northern (6.1 m/km; $R^2 = 0.621$; RMSE = 134; Figure 5d) and southern (3.8 m/km; $R^2 = 0.548$; RMSE = 155; Figure 6d) regions. For both CFAs and modern cirque glacier ELAs, the relationship with distance to the coastline is stronger in the northern region (where cirques and glaciers are also typically closer to the coast) than in the southern region. The inland increase in CFAs and modern cirque glacier ELAs follows the overall topographic gradient of the Scandinavian Mountains, with elevations increasing inland. These data illustrate that in each region, distance from the modern coastline is the individual variable that shows the strongest relationship with CFA (as indicated by R^2 and RMSE). In each region, multiple regression of CFA against latitude, longitude and distance from the modern coastline returns the highest R^2 and lowest RMSE. However, distance from the modern coastline dominates these relationships (i.e. it is consistently the variable with the strongest *t* value), and they only differ slightly from those based on CFA and distance from the coastline alone (Table 3).

5.0 DISCUSSION

Cirque morphology, aspect, and elevation, including CFAs, are thought to represent a time-transgressive record of climatic and glaciological conditions during former periods when cirques were occupied periodically by erosive (warm-based) ice (Meierding, 1982; Barr and Spagnolo, 2013; Ipsen et al., 2017). These conditions occurred multiple times during the Quaternary (and pre-Quaternary) in Scandinavia, but usually towards the onset and termination of each glacial cycle. By contrast, modern cirque glacier ELAs only (or largely) reflect climatic conditions at a single period in time (i.e., the present), when glaciers are experiencing generalised retreat. Given this difference, here we discuss the factors that potentially control CFAs and modern cirque glacier ELAs and assess if, and how, these differ. From this, we consider what CFAs can tell us about palaeoclimate.

5.1. Factors controlling CFAs and modern cirque glacier ELAs

5.1.1. Climate

Across the study region, the northward decline in CFAs and modern cirque glacier ELAs (Figure 4a), although to some degree a function of the two sub-regions, suggests that a latitudinal decline in air temperatures played a role in regulating the altitude at which former mountain glaciers were

able to initiate (generating cirques) and regulates where cirque glaciers are currently able to exist (Renseen et al., 2001; Fredin, 2002; Ipsen et al., 2017). However, since this latitudinal decline in CFAs is far less apparent when sub-populations (i.e., northern and southern) are considered (Figure 5a & 6a), it is likely that this control mostly operates over large spatial scales (Bakke et al., 2008). More locally, there is evidence that topographic sheltering and/or shading (as reflected by cirque and cirque glacier aspects) plays a role in regulating CFAs and modern ELAs, suggesting that glacier initiation and sustenance was/is promoted at lower altitudes on east-facing slopes (Figure 8) (Olyphant, 1977; Hassinen, 1998).

Despite the evidence for air temperature and aspect-related controls, the strongest region-wide pattern in both CFAs and modern cirque glacier ELAs is an increase with distance inland, which corresponds to present-day prevailing wind direction (W/SW to E/NE). Similar inland trends are found in other regions and are thought primarily to reflect a limit to favourable glacial conditions, imposed by a gradual inland reduction in precipitation (Peterson and Robinson, 1969; Nesje et al., 2008; Principato and Lee, 2014; Barr and Spagnolo 2015a; Barr et al., 2017; Ipsen et al., 2018; Wallick and Principato, 2020). In Scandinavia specifically, this logic implies that, exposure to moisture from the Norwegian Sea is a key factor controlling former sites of glacier initiation and modern glacier ELAs (Bakke et al., 2008; Nesje et al., 2008; Evans, 2011; Oien et al., 2020). Present-day precipitation shows a strong relationship with modern cirque glacier ELAs in Scandinavia (Winkler et al., 2009; Oien et al., 2020). Our CFA study suggests that palaeoprecipitation gradients similar to present-day might have existed during periods of the Quaternary (or earlier) when cirques formed and were subsequently re-occupied by cirque glaciers. This long-term stability of climatic gradients in the region has been suggested previously, as other palaeoclimatic proxies have shown, for example, that maritime wet conditions were recurrent throughout the Holocene in the coastal part of the southern region of Scandinavia (Seppä and Birks, 2001; Bjune et al., 2005; Bakke et al., 2008). Furthermore, palaeoclimate models, extending through the last glaciation maximum and Younger Dryas, show an overall pattern of precipitation decreasing inland (e.g. Ressen et al., 2001; Forsström, 2005; Rea et al., 2020).

For the region as a whole, and the two sub-regions, the inland increase in CFAs has a slightly steeper gradient than the increase in modern ELAs. Barr and Spagnolo (2015b) found a similar trend between CFAs and modern glacier ELAs in Kamchatka (Eastern Russia). They attributed this difference to the fact that CFAs reflect sites of former glacier initiation (largely controlled by

snowfall), while modern glacier ELAs are also strongly regulated by the variety of topoclimatic factors which control ablation (i.e., the link to precipitation is weakened, and modern glaciers can survive even in regions with limited snowfall). This difference in the factors controlling CFAs and modern ELAs might also apply in Scandinavia. However, it is also possible that the steeper inland CFA gradient (when compared to modern glacier ELAs) in Scandinavia reflects the control of ice sheet growth on areas suitable for cirque formation (see Section 5.1.3).

5.1.2. Topography

Topographic availability exerts a control on where glaciers can develop, e.g. high-altitude glaciers can only form where high-altitude topography exists. Therefore, regional trends in CFAs and modern glacier ELAs likely partly reflect topographic (i.e. mountain elevation) gradients. Oien et al (2020) considered the potential role of topography in controlling modern cirque glacier ELAs across Scandinavia and found that mean topography and modern ELAs increase inland with similar gradients. Results from the present study reveal that CFAs also increase inland, with very similar (but slightly steeper) gradients. Studies in other regions globally have contemplated the possible role that topographic gradients play in regulating CFAs (e.g., Peterson and Robinson, 1969; Hassinen, 1998; Dahl and Nesje, 1992; Anders et al., 2010; Mitchell and Humphries, 2014; Barr and Spagnolo, 2015b; Barr et al., 2017; Wallick and Principato, 2020). Though these studies acknowledge the role of topography, most conclude by suggesting that palaeoprecipitation gradients (as indicated by cirque distance from the coast) are likely the dominant control on CFAs. In Scandinavia specifically, Hassinen (1998), focusing on an area at the very north of our study, considered the inland increase in CFAs to reflect palaeoprecipitation gradients combined with topographic trends (i.e., mountain heights gradually increase to the east, but at a slower rate than CFAs). Similarly, Oien et al. (2020) concluded that inland precipitation reduction and topographic gradients likely act together to regulate modern cirque glacier ELAs in the Scandinavian Mountains. The results from the present study support the idea that, as with modern cirque glacier ELAs, trends in CFAs are, to some degree, dictated by topography. This is illustrated in Figure 9, which suggests that neither ELA gradients nor topographic gradients alone can explain the inland cirque distribution observed in Scandinavia. The former fails to explain the absence of high-altitude cirques near the coast (Figure 9a), and the latter fails to explain the absence of low-altitude

314 cirques further inland (Figure 9b). However, when both inland ELA gradients and topographic
315 gradients are considered, observed CFA trends are understandable (Figure 9c).
316
317 5.1.3. *Glacial history*
318
319 During glacial periods, large ice masses readily develop in the Scandinavian Mountains and
320 coalesce to form an ice sheet (e.g. Mangerud, 2008; Mangerud et al., 2011; Fredin et al., 2013;
321 Olsen et al., 2013a; Hughes et al., 2016). In Scandinavia, these large ice masses first occupy the
322 highest mountains of the interior of the southern region, and gradually advance and coalesce to
323 cover the entire peninsula (Fredin, 2002; Kleman et al., 2008; Mangerud et al., 2011; Olsen et al.,
324 2013a; Olsen et al., 2013b). Once a landscape is submerged by ice, 'new' cirques cannot form and
325 existing cirques experience minimal modification. Thus, in interior locations (i.e., far from the
326 coast), the formation of 'new', and modification of existing, cirques likely stop comparatively
327 early during the onset of glacial periods (when the local ELA is still relatively high), since the
328 landscape quickly becomes entirely submerged by largely cold-based (i.e. non erosive) ice
329 extending from local high-altitude regions of ice-sheet initiation. By contrast, in coastal locations
330 the local ELA may drop close to sea level (as indicated by CFAs), before the landscape is
331 submerged by an ice sheet (Rudberg, 1994; Dahl et al., 1997; Hassinen, 1998; Nesje, 2009).
332 This means that in Scandinavia low-altitude cirques can only develop in coastal locations, and not
333 in interior regions. It is reasonable to assume that the lowest elevation cirques, particularly those
334 along the modern-day coast in the northern region (Figure 3a), would only be filled at times of
335 extensive glaciation (Agrell, 1977; Olyphant, 1977; Dahl et al., 1997; Batchelor et al., 2019). This
336 spatial difference in glacial history is likely to enhance the inland trend in CFAs (already dictated
337 by climate and topography – see sections 5.1.1., and 5.1.2.) (Figure 9d) and might help explain
338 why inland gradients in CFAs are slightly steeper than modern ELA gradients.
339
340 5.1.4. *Additional factors*
341 In previous studies elsewhere, spatial variations in glacio-isostatic adjustment and former glacial
342 erosion rates (linked to ice dynamics and subglacial geology) have been considered as possible
343 explanations for region-wide trends in CFA (e.g., Bakke et al., 2005; Barr and Spagnolo, 2015b;
344 Barr et al., 2017). However, in Scandinavia, there is little evidence to suggest that these factors

control the trends in CFAs. For example, all the cirques analysed in this study are currently experiencing glacio-isostatic uplift (Rosentau et al., 2012), and those in interior regions are experiencing more rapid and greater uplift than in coastal locations (Rosentau et al., 2012). This means that cirques in interior locations may be further below the altitude at which they formed than is the case for coastal cirques. If so, correcting CFAs for residual glacial isostatic adjustment would increase the inland gradient. In fact, glacial isostatic adjustment may help partly explain why the inland gradient in CFAs is steeper than for modern ELAs, since the former may have been affected by differential uplift since deglaciation, while the latter reflects the contemporary climate and is therefore independent of isostatic adjustment.

While there is regional variability in cirque lithology, there are no broad-scale trends to suggest that bedrock resistance increases with distance from the coast, certainly not in any way that explains overall trends in CFAs (unlike Delmas et al., 2014; Delmas et al., 2015). Finally, the dynamics of former cirque glaciers may have varied regionally, and there is evidence to indicate that coastal glaciers may have been more dynamic (with higher mass turnover). Additionally, the coastal, low-elevation glaciers would have only been covered by the ice sheet at maximum extent, and may have experienced greater time of active cirque glacier occupation than those in the interior that would have been shielded by cold-based ice (Olsen et al., 2001; Bakke et al., 2005; Batchelor et al., 2019). Any spatial differences in glacier dynamics are likely to result in differences in CFAs on the order of tens of metres (e.g. Dahl et al., 1997; Barr et al., 2017), not the hundreds of metres difference between the coast and peak mountains as observed.

5.2. Limitations of CFAs as palaeoclimate indicators

As outlined above, when glaciers are small, and largely confined to their cirques (i.e., during periods of cirque glaciation), CFAs roughly approximate cirque glacier ELAs, and could therefore be used (with some caveats) as a source of quantitative palaeoclimate information (precipitation and/or temperature). However, this palaeoclimatic information only becomes useful when it can be assigned to a particular time period. This requires geochronometric dating to establish when cirque-confined glaciers last occupied a landscape. This is possible through surface exposure dating (e.g., Barth et al., 2016; Barth et al., 2017), but it is expensive and impractical to apply to large populations, particularly when (as in the present study) thousands of

cirques are considered. Without chronological information for many cirques, the palaeoclimatic inferences that can be drawn from populations are limited. Despite this caveat, trends in CFA may reflect general, long-lasting or recurrent palaeoclimatic gradients – i.e. compound (palimpsest) gradients from the superimposition of several glacial phases. However, where CFAs track topography (as in the present study), isolating and quantifying the climatic component is difficult. Where CFA trends differ from modern ELA or climate trends, this might indicate changing climate (i.e., precipitation) patterns through time (e.g., Evans, 1999). However, in almost all cases, trends in CFA generally track modern climate/ELA (Peterson and Robinson, 1969; Hassinen, 1998; Anders et al., 2010; Barr and Spagnolo, 2015b; Barr et al., 2017; Wallick and Principato, 2020), and obtaining any useful palaeoclimatic information (beyond establishing that broad precipitation gradients have changed little through time – as observed in the present study) relies on interpreting differences between the two (e.g., Barr and Spagnolo, 2015b). However, in Scandinavia, even extracting palaeoclimatic information in this way is complicated by the potential role that the glacial history has played in regulating CFAs (Section 5.1.3.).

6.0 CONCLUSIONS

In this study, 3984 cirque floor altitudes (CFAs) and 513 modern cirque glacier ELAs were analysed across the Scandinavian Peninsula. We investigated trends in these data to establish controls on past and present glaciers in the region, and to establish what palaeoclimatic information can be obtained from CFAs. The main study findings are:

1. Latitudinal and aspect-related trends in CFA and modern glacier ELAs suggest that air temperatures and local shading played, and continue to play, a role in regulating sites of mountain glaciation across the Scandinavian Peninsula.
2. The dominant trend in CFAs and modern glacier ELAs across the region is an increase inland i.e., increasing with distance from the coast. These trends likely reflect the combined influence of climatic gradients (controlling past and present ELAs), and topographic gradients (restricting where glaciers and cirques can form). In the case of CFAs, unravelling controls on the increase inland is further complicated by spatial differences in glacial history (in particular, ice sheet growth in the interior during glacial periods, preventing the formation of low altitude cirques).

3. Results from the present study, supported by other studies, suggest that individual CFAs can yield useful (quantitative), but limited, palaeoclimate information. However, given the potential role of climate, topography, and glacial history (and the difficulties with disentangling these controls), palaeoclimatic interpretations derived from cirque populations and/or CFA trends should be treated with caution.

7.0 ACKNOWLEDGEMENTS

The Scottish Alliance for Geoscience Environment and Society (SAGES) and the University of Aberdeen are thanked for funding the PhD studentship awarded to Rachel P. Oien. I am grateful for the data provided by various scientists at the NVE and NGU in order to make this project possible. We thank Ian Evans, and an anonymous reviewer for their extremely helpful corrections, comments, and suggestions.

8.0 FIGURES

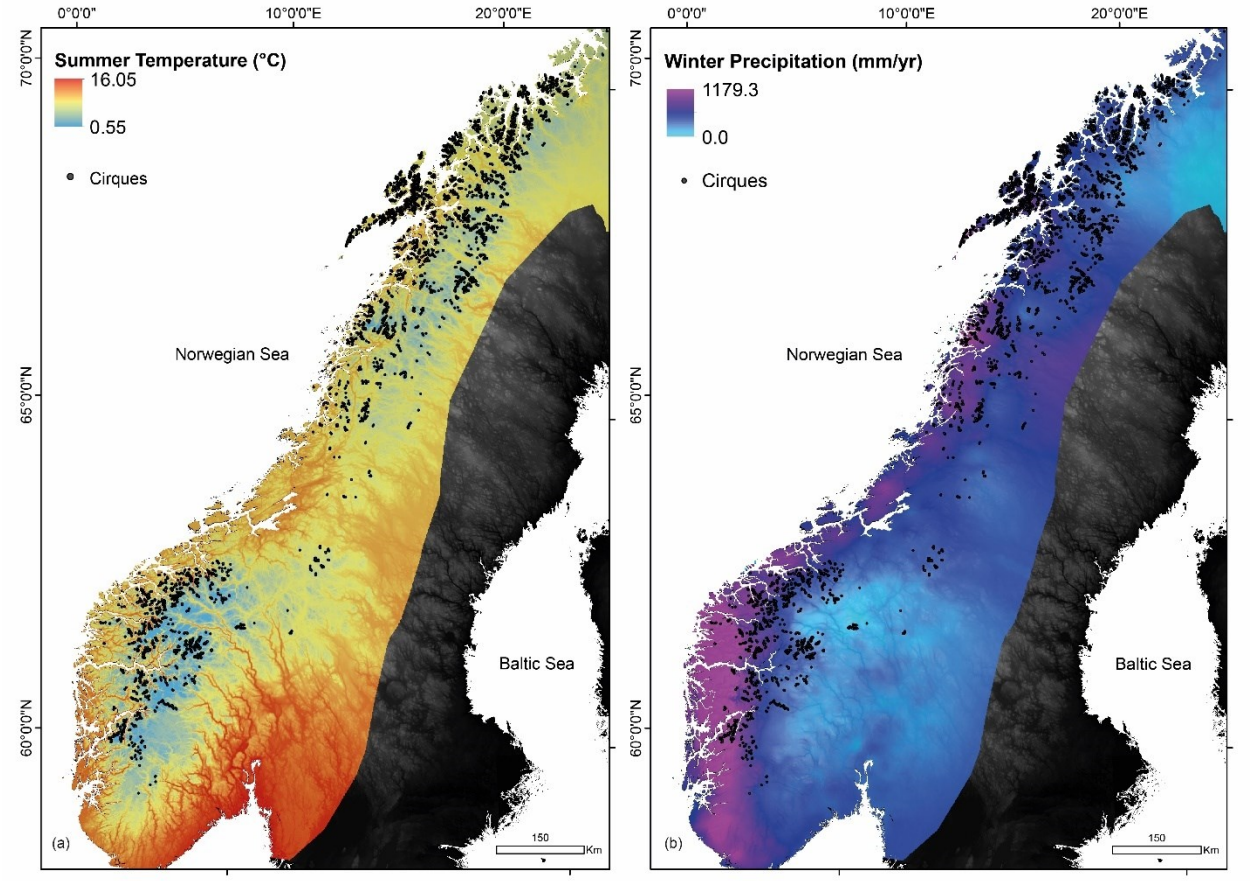

Figure 1. (a) Mean summer air temperature (JJA) and (b) total winter precipitation (DJF) patterns for present-day Scandinavia (NVE, 2017). Winter precipitation and summer temperatures are averaged over 30 years from 1971-2000 (NVE, 2017).

Figure 2. An example of two of the mapped glacier-free cirque outlines (in pink) overlayed in Google Earth, located at 62°28'43.97"N 7°57'41.59"E.

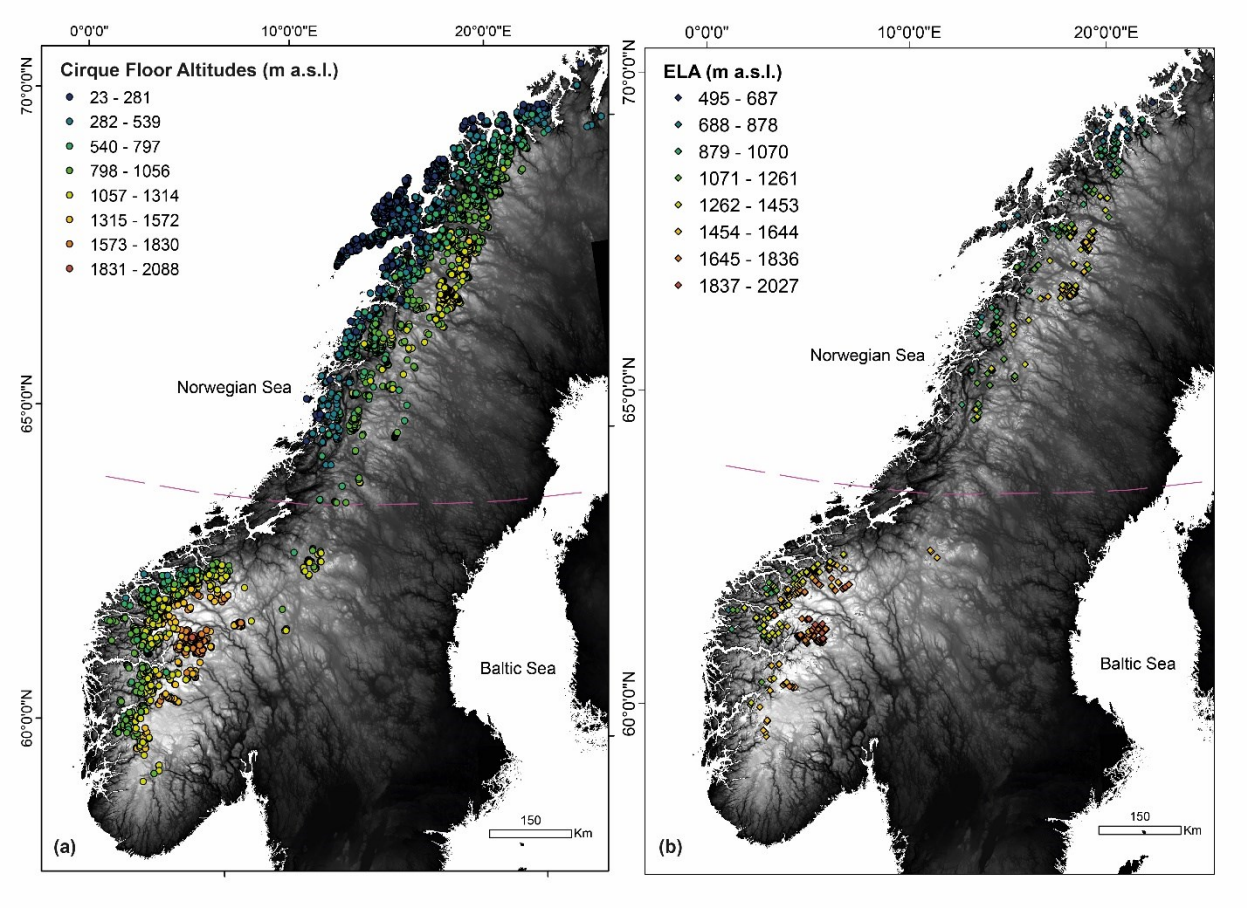

Figure 3. (a) Cirque floor altitudes and (b) modern-glacier ELAs. The dashed line separates regions termed in the text as the northern and southern regions.

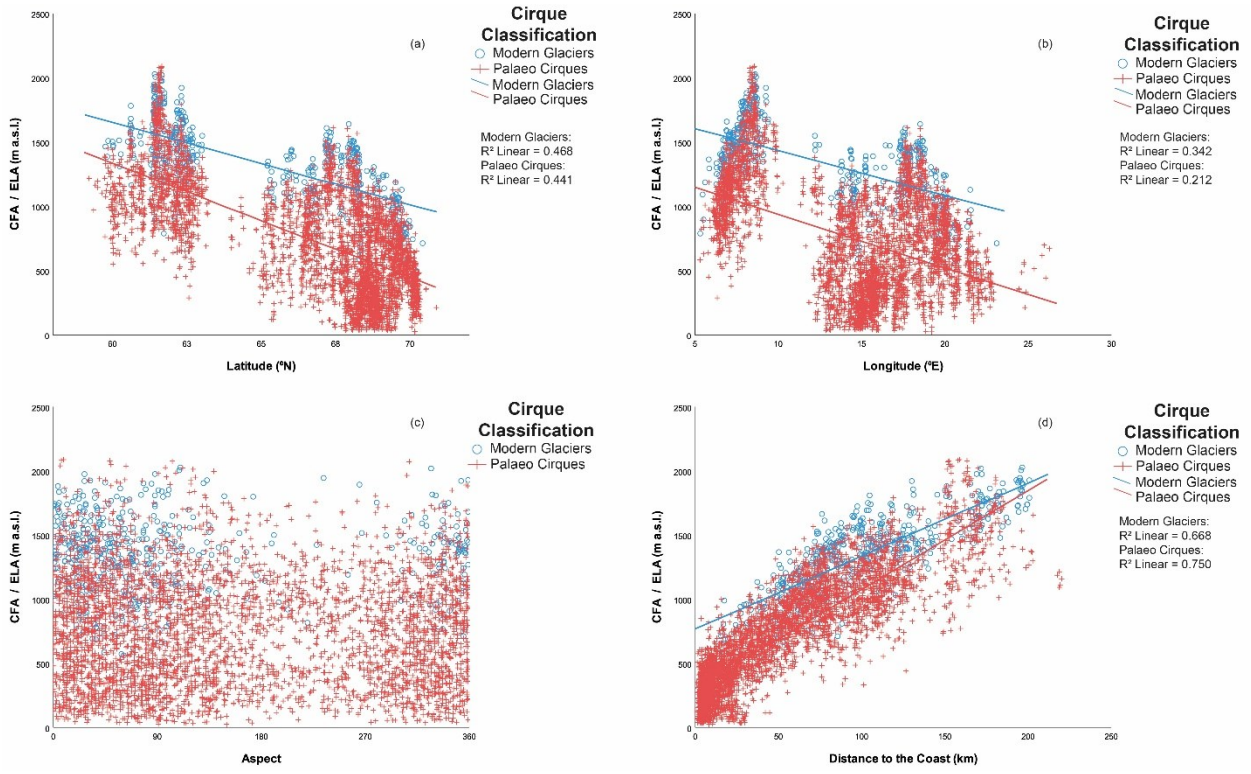

Figure 4. Variations in cirque floor altitudes and glacier ELAs, with: (a) latitude; (b) longitude; (c) aspect; and (d) distance to the modern coastline.

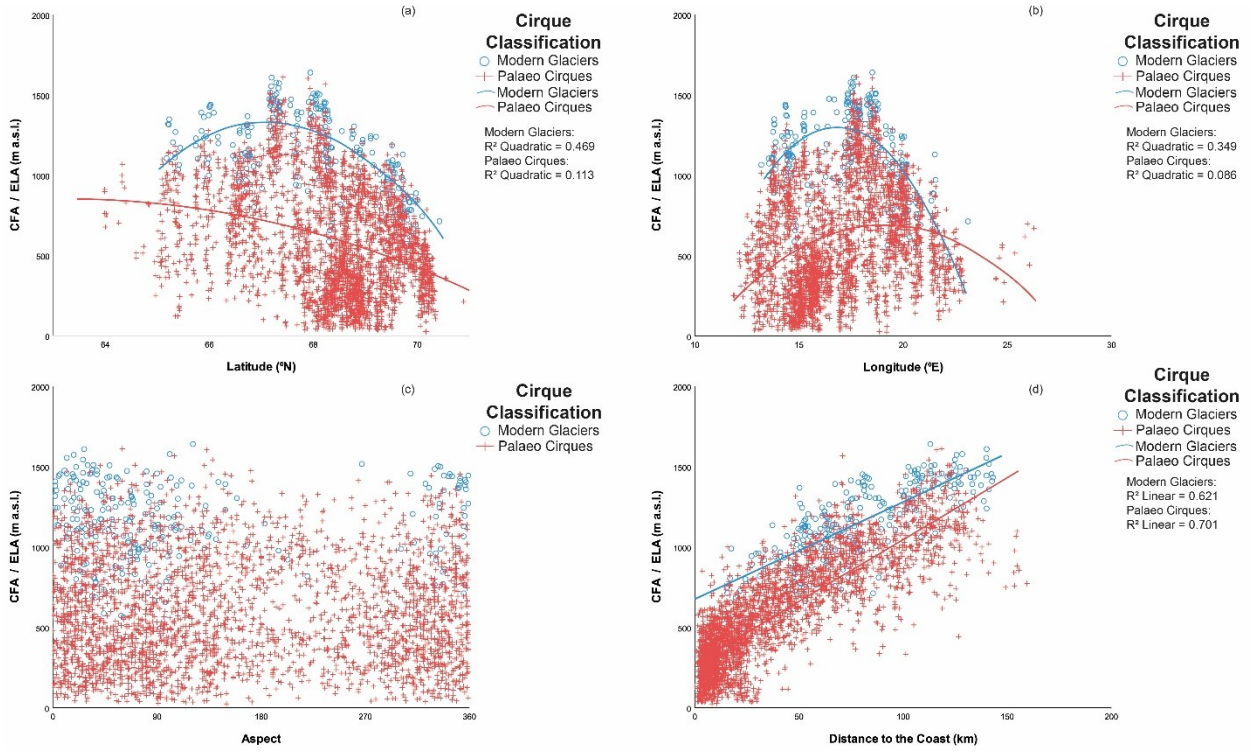

Figure 5. Variations in cirque floor altitudes and glacier ELAs in the northern region with: (a) latitude; (b) longitude; (c) aspect; (d) distance to the modern coastline.

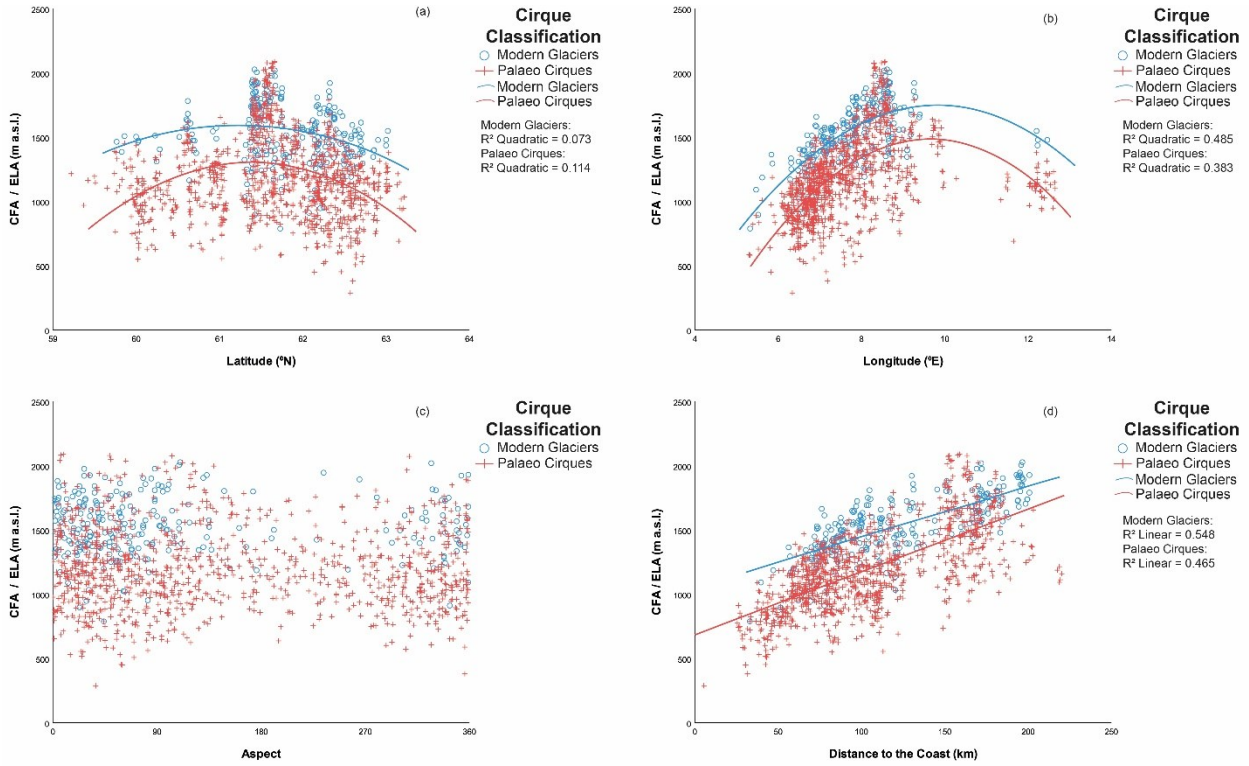

452

453 Figure 6. Variations in cirque floor altitudes and glacier ELAs in the southern region with: (a)

454 latitude; (b) longitude; (c) aspect; (d) distance to the modern coastline.

455

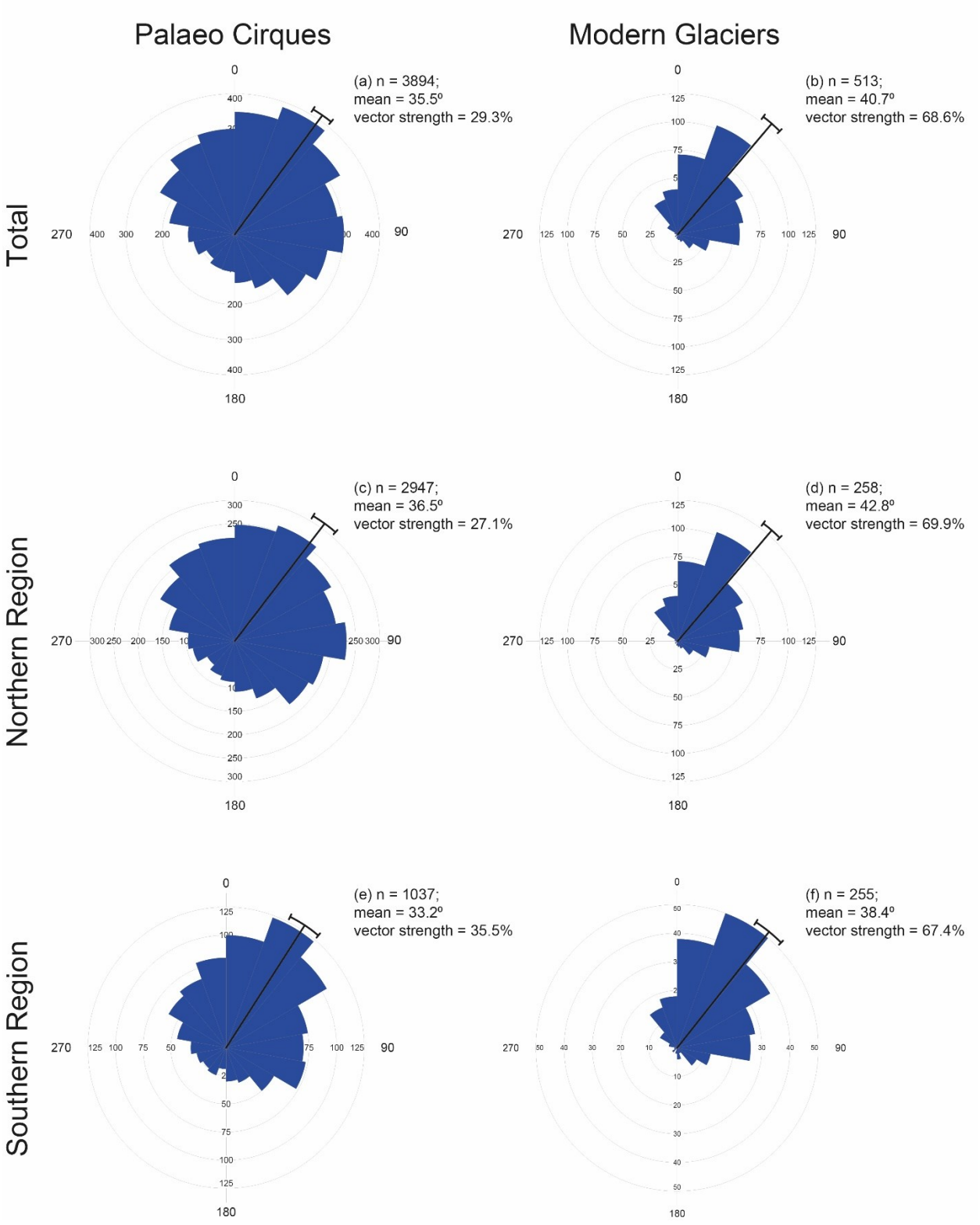

Figure 7. Rose diagrams (linear scale of frequency with equal bin widths) of mean vector aspect frequency and vector strength. (a) Entire cirque population, (b) entire modern cirque glacier

population, (c) cirques in the northern region, (d) modern cirque glaciers in the northern region, (e) cirques in the southern region, (f) modern cirque glaciers in the southern region. In each Rose diagram, the line represents the vector mean and the bar (on the end of each line) shows the 95% confidence interval.

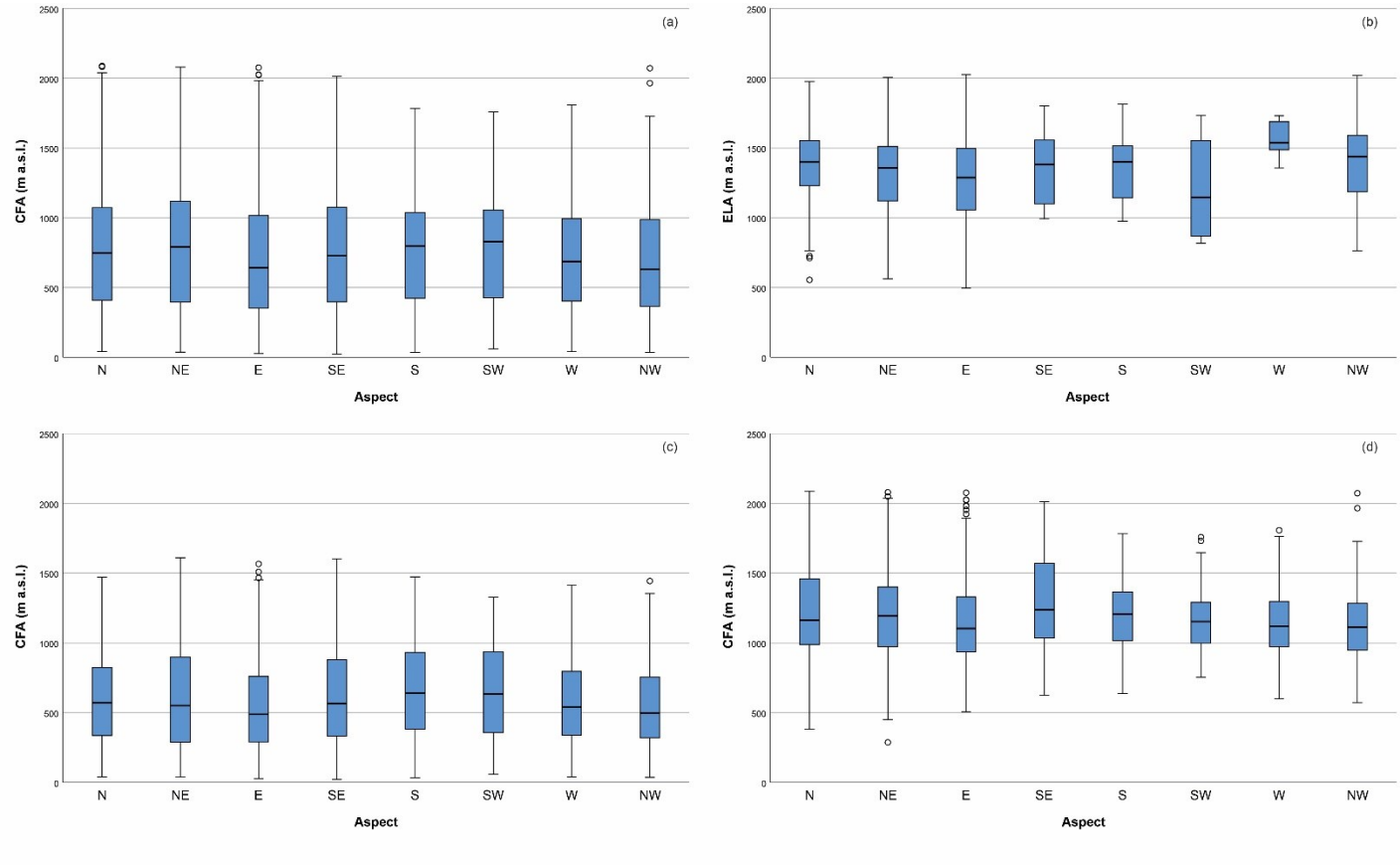

Figure 8. Boxplots comparing the CFA or ELA with aspect for the (a) whole cirque dataset (b) modern cirque glaciers (c) northern cirque region (d) southern cirque region. The thick middle line indicates the median, the top and bottom of the box represent the 1st and 3rd quartiles and the edge of the whisker represent the range, maximum and minimum excluding outliers. Outliers (open circles) are defined as points which lie more than 1.5 box lengths beyond the interquartile range. The number of modern glaciers and cirques within each aspect group is shown in Table 4.

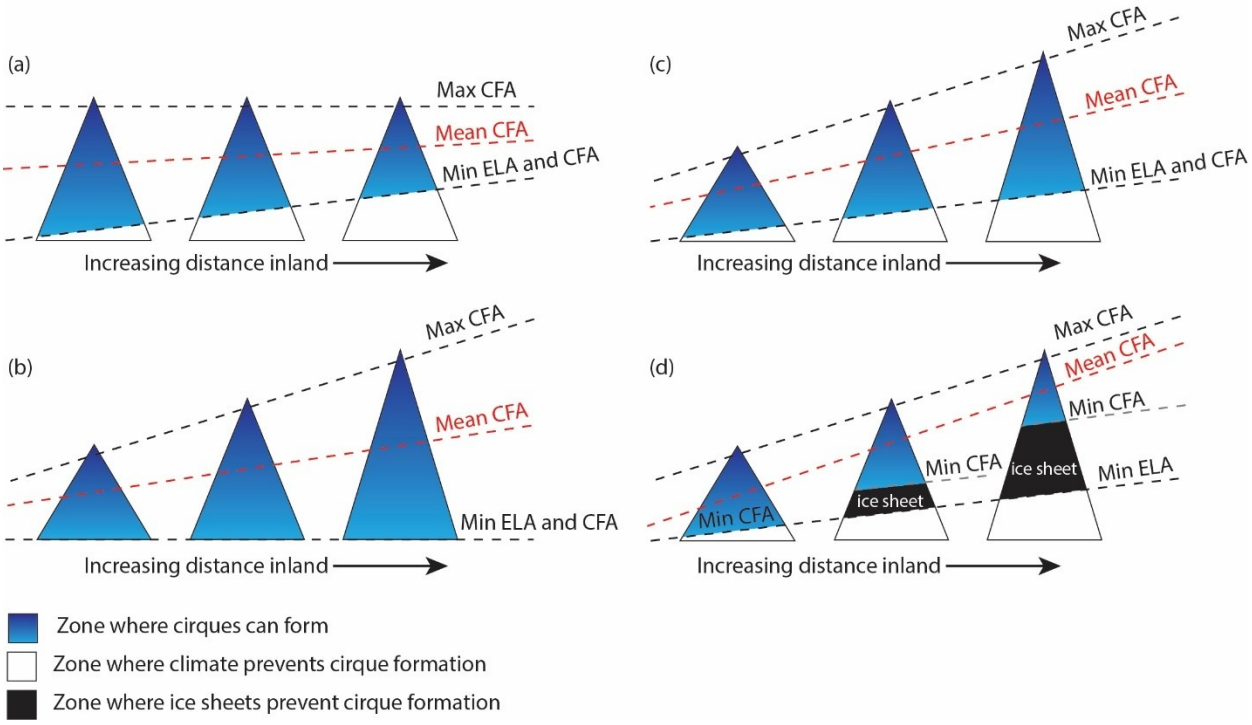

Figure 9. Schematic illustration of potential drivers of the inland increase in minimum, mean and maximum CFAs observed in the present study. (a) Climatic gradient alone (as indicated by variability in climatic ELA), (b) topographic gradient alone, (c) climatic and topographic gradients, (d) climatic and topographic gradients, combined with spatial variability in glacial history, with the top of the black margin representing the minimum CFA (i.e., the formation of ice sheets at inland locations) and the bottom the minimum ELA. This illustration indicates that only scenarios (c) and (d) produce CFA distributions comparable to that seen in Figure 4d, despite the complex history of uplift in the Scandinavian Mountains (Nielsen et al., 2009; Steer et al., 2012; Pedersen, et al., 2021).

9.0 TABLES

Table 1: Cirque floor altitudes (cirques) and ELAs (modern mountain glaciers) across the Scandinavian Peninsula, subdivided by region.

	Total Population (cirques)	Northern Region (cirques)	Southern Region (cirques)	Total Population (glaciers)	Northern Region (glaciers)	Southern Region (glaciers)

Number:	3984	2947	1037	513	258	255
Min (m a.s.l.)	23	23	287	495	495	788
Max (m a.s.l.)	2088	1610	2088	2027	1639	2027
Mean (m a.s.l.)	745	591	1195	1339	1151	1528
Median (m a.s.l.)	721	541	1166	1368	1158	1519
Std. dev (m a.s.l.)	422	333	311	303	245	229

Table 2: Summary statistics for the CFAs/ELAs and distance to the coast within the northern and southern regions for cirques and modern glaciers. All characteristics were extracted using ACME (Spagnolo et al., 2017).

	Northern Cirques (n = 2947)			Northern Modern Glaciers (n = 258)		
	Mean	Median	Std. Deviation	Mean	Median	Std. Deviation
CFA/ELA (m a.s.l.)	591	541	333	1151	1158	245
Distance to the Coast (km)	40.83	27.01	36.3	67.73	64.97	33.16
	Southern Cirques (n = 1037)			Southern Modern Glaciers (n = 255)		
	Mean	Median	Std. Deviation	Mean	Median	Std. Deviation
CFA/ELA (m a.s.l.)	1195	1166	311	1528	1519	229
Distance to the Coast (km)	104.67	96.98	43.32	108.18	97.65	42.09

Table 3. Regression of cirque floor altitude (CFA) against latitude (Lat), longitude (Lon), distance from the modern coastline (D), and aspect (α). Significant relationships (i.e., where $p < 0.01$*, $p<0.05$**), other than those based on multiple regression, are shown in Figs 3-5. For equations based on multiple regression, the coefficient and variable with the strongest *t* value are in **bold**.

Region	**Variable**	**Equation**	**p-value**	**R^2**	**RMSE (m)**
Total	Lat	CFA = -88.74Lat + 6659.64	<0.01*	0.441	315
	Lon	CFA = -41.63Lon + 1356.03	<0.01*	0.212	374
	Dist (D)	CFA = 7.70D + 305.86	<0.01*	0.750	211
	Aspect (α)	Not stat. sig.	0.31	n/a	n/a
	Lat, lon, dist (D)	CFA = -85.40Lat + 35.78Lon + **5.49D** + 5598	<0.01*	0.778	199
Northern	Lat	CFA = -9.60Lat^2 + 1215.10Lat - 37603	<0.01*	0.113	314
	Lon	CFA = -8.95Lon^2 + 342.36Lon - 2586	<0.01*	0.086	319
	Dist (D)	CFA = 7.69D + 277	<0.01*	0.701	182
	Aspect (α)	CFA = -23.90cosα -1.24sinα + 596.45	0.03**	n/a	n/a
	Lat, lon, dist (D)	CFA = -108.46Lat + 51.38Lon + **5.58D** + 6902	<0.01*	0.731	174
Southern	Lat	CFA = -135.14Lat^2 + 16589Lat - 507781	<0.01*	0.114	293
	Lon	CFA = -53.38Lon^2 + 1030.40Lon – 3489	<0.01*	0.383	244
	Dist (D)	CFA = 4.90D + 682	<0.01*	0.465	227
	Aspect (α)	Not stat. sig.	0.06	n/a	n/a
	Lat, lon, dist (D)	CFA = 121.92Lat – 65.04Lon + **6.54D** – 6505	<0.01*	0.503	219

Table 4. Number of modern glaciers and cirques within each aspect group. N, 337.5–22.5°; NE, 22.5–67.5°; E, 67.5–112.5°; SE, 112.5–157.5°; S, 157.5–202.5°; SW, 202.5–247.5°; W, 247.5–292.5°; NW, 292.5–337.5

	N	NE	E	SE	S	SW	W	NW
Modern glaciers (total)	136	181	114	25	10	4	6	37
Modern glaciers (North)	67	88	64	13	4	2	1	19

Modern glaciers (South)	69	93	50	12	6	2	5	18
Cirques (total)	742	779	629	477	263	233	316	545
Cirques (North)	527	534	475	371	210	176	237	417
Cirques (South)	215	245	154	106	53	57	79	128

511
512
513
514

515 **10.0 REFERENCES**

516 Agrell, H. (1977). A Glacial Cirque Form in Central Sweden? *Geografiska Annaler*, Series A:
517 Physical Geography, 59(3/4), 215–219.

518 Anders, A. M., Mitchell, S. G., & Tomkin, J. H. (2010). Cirques, peaks, and precipitation
519 patterns in the Swiss Alps: Connections among climate, glacial erosion, and topography.
520 *Geology*, 38(3), 239–242. https://doi.org/10.1130/G30691.1

521 Argus, D. F., & Peltier, W. R. (2010). Constraining models of postglacial rebound using space
522 geodesy: a detailed assessment of model ICE-5G (VM2) and its relatives. *Geophys. J. Int*, 697–
523 723. https://doi.org/10.1111/j.1365-246X.2010.04562.x

524 Bacon, S. N., Chinn, T. J., Van Dissen, R. J., Tillinghast, S. F., Goldstein, H. L., & Burke, R. M.
525 (2010). New Zealand Journal of Geology and Geophysics Paleo-equilibrium line altitude
526 estimates from late Quaternary glacial features in the Inland Kaikoura Range, South Island, New
527 Zealand. *New Zealand Journal of Geology and Geophysics*, 44(1), 55–67.
528 https://doi.org/10.1080/00288306.2001.9514922

529 Bakke, J., Dahl, S. O., Paasche, Ø., Løvlie, R., & Nesje, A. (2005). Glacier fluctuations,
530 equilibrium-line altitudes and palaeoclimate in Lyngen, northern Norway, during the Lateglacial
531 and Holocene. *The Holocene*, 15(4), 518–540. https://doi.org/10.1191/0959683605hl815rp

532 Bakke, J., Lie, Ø., Dahl, S. O., Nesje, A., & Bjune, A. E. (2008). Strength and spatial patterns of
533 the Holocene wintertime westerlies in the NE Atlantic region. *Global and Planetary Change*,
534 60(1–2), 28–41. https://doi.org/10.1016/j.gloplacha.2006.07.030

535 Barr, I. D., & Spagnolo, M. (2013). Palaeoglacial and palaeoclimatic conditions in the NW
536 Pacific, as revealed by a morphometric analysis of cirques upon the Kamchatka Peninsula.
537 *Geomorphology*, 192, 15–29. https://doi.org/10.1016/j.geomorph.2013.03.011

Barr, I. D., & Spagnolo, M. (2015a). Understanding controls on cirque floor altitudes: Insights from Kamchatka. *Geomorphology*, 248, 1–13. https://doi.org/10.1016/j.geomorph.2015.07.004

Barr, I. D., & Spagnolo, M. (2015b). Glacial cirques as palaeoenvironmental indicators: Their potential and limitations. *Earth-Science Reviews*, 151(0), 48–78. https://doi.org/10.1016/j.earscirev.2015.10.004

Barr, I. D., Ely, J. C., Spagnolo, M., Clark, C. D., Evans, I. S., Pellicer, X. M., and Rea, B. R. (2017). Climate patterns during former periods of mountain glaciation in Britain and Ireland: Inferences from the cirque record. *Palaeogeography, Palaeoclimatology, Palaeoecology*, 485, 466–475. https://doi.org/10.1016/j.palaeo.2017.07.001

Barth, A. M., Clark, P. U., Clark, J., McCabe, A. M., & Caffee, M. (2016). Last Glacial Maximum cirque glaciation in Ireland and implications for reconstructions of the Irish Ice Sheet. *Quaternary Science Reviews*, *141*, 85–93. https://doi.org/10.1016/j.quascirev.2016.04.006

Barth, A. M., Clark, P. U., Clark, J., Roe, G. H., Marcott, S. A., Marshall McCabe, A., Caffee, M.W., He, F., Cuzzone, J.K., and Dunlop, P. (2018). Persistent millennial-scale glacier fluctuations in Ireland between 24 ka and 10 ka. *Geology*, *46*(2), 151–154. https://doi.org/10.1130/G39796.1

Batchelor, C. L., Margold, M., Krapp, M., Murton, D. K., Dalton, A. S., Gibbard, P. L., Stokes, C. R., Murton, J. B., and Manica, A. (2019). The configuration of Northern Hemisphere ice sheets through the Quaternary. *Nature Communications*. https://doi.org/10.1038/s41467-019-11601-2

Benn, Douglas I.; Lehmkuhl, F. (2000). Mass balance and equilibrium-line altitudes of glaciers in high-mountain environments. *Quaternary International*, 65/66, 15–29.

Bjune, A. E., Bakke, J., Nesje, A., & Birks, H. J. B. (2005). Holocene mean July temperature and winter precipitation in western Norway inferred from palynological and glaciological lake-sediment proxies. *The Holocene*, 15(2), 177–189.

Caseldine, C., & Stotter, J. (1993). "Little Ice Age'' glaciation of Trollaskagi peninsula, northern Iceland: climatic implications for reconstructed equilibrium line altitudes (ELAs)." *The Holocene*, 3(4), 357–366. https://doi.org/10.1177/095968369300300408

Coleman, C. G., Carr, S. J., & Parker, A. G. (2009). Modelling topoclimatic controls on palaeoglaciers: implications for inferring palaeoclimate from geomorphic evidence. *Quaternary Science Reviews*, 28(3–4), 249–259. https://doi.org/10.1016/j.quascirev.2008.10.016

Dahl, S. O., & Nesje, A. (1992). Paleoclimatic implications based on equilibrium-line altitude depressions of reconstructed Younger Dryas and Holocene cirque glaciers in inner Nordfjord, western Norway. In *Palaeogeography, Palaeoclimatology, Palaeoecology* (Vol. 94).

572 Dahl, S. O., Nesje, A., & Øvstedal, J. (1997). Cirque glaciers as morphological evidence for a
573 thin Younger Dry as ice sheet in east-central southern Norway. *Boreas*, 26(3), 161–180.
574 https://doi.org/10.1111/j.1502-3885.1997.tb00850.x

575 Delmas, M., Gunnell, Y., & Calvet, M. (2014). Environmental controls on alpine cirque size.
576 *Geomorphology*, 206, 318–329. https://doi.org/10.1016/j.geomorph.2013.09.037

577 Delmas, M., Gunnell, Y., & Calvet, M. (2015). A critical appraisal of allometric growth among
578 alpine cirques based on multivariate statistics and spatial analysis. *Geomorphology*, 228, 637–
579 652. https://doi.org/10.1016/j.geomorph.2014.10.021

580 Etzelmüller, B., Romstad, B., & Fjellanger, J. (2007). Automatic regional classification of
581 topography in Norway. In *Norwegian Journal of Geology* (Vol. 87).

582 Evans, I. S. (1977). World-Wide Variations in the Direction and Concentration of Cirque and
583 Glacier Aspects. *Geografiska Annaler, Series A: Physical Geography*, *59*(3/4), 151–175.
584 https://doi.org/https://www.jstor.org/stable/520797

585 Evans, I. S. (1999). Was the cirque glaciation of Wales time-transgressive, or not? *Annals of*
586 *Glaciology*, 28, 33–39. https://doi.org/10.3189/172756499781821652

587 Evans, I.S., 2006a. Local aspect asymmetry of mountain glaciation: a global survey of
588 consistency of favoured directions for glacier numbers and altitudes. *Geomorphology* 73, 166–
589 184.
590

591 Evans, I. S. (2006b). Glacier Distribution in the Alps : Statistical Modelling of Altitude and
592 Aspect. *Geografiska Annaler, Series A: Physical Geography*, 88 A(2), 115–133.
593 https://doi.org/10.1111/j.0435-3676.2006.00289.x

594
595 Evans, I.S., (2011). Glacier distribution and direction in Svalbard, Axel Heiberg Island
596 and throughout the Arctic: general northward tendencies. *Polish Polar Res.* 32, 199–238.
597
598 Evans, I.S., Cox, N., (1974). Geomorphometry and the operational definition of cirques. *Area*
599 6 (2), 150–153.
600

601 Fredin, O. (2002). Glacial inception and Quaternary mountain glaciations in Fennoscandia.
602 *Quaternary International*, 95–96, 99–112. https://doi.org/10.1016/S1040-6182(02)00031-9

603 Forsström, P.-L. (2005). Through a glacial cycle: simulation of the Eurasian ice sheet dynamics
604 during the last glaciation. *Annales Academiae Scientiarum Fennicae Geologica-Geographica*,
605 168, 1–94.

606 Hassinen, S. (1998). A morpho-statistical study of cirques and cirque glaciers in the Senja-
607 Kilpisjärvi area, northern Scandinavia. *Norsk Geografisk Tidsskrift-Norwegian Journal of*
608 *Geography*, 52(1), 27–36. https://doi.org/10.1080/00291959808552381
609

610 Hughes, P. D. (2010). Little Ice Age glaciers in the Balkans: Low altitude glaciation enabled by
611 cooler temperatures and local topoclimatic controls. *Earth Surface Processes and Landforms*,
612 *35*(2), 229–241. https://doi.org/10.1002/esp.1916

613 Hughes, A. L. C., Gyllencreutz, R., Lohne, Ø. S., Mangerud, J., & Svendsen, J. I. (2016). The
614 last Eurasian ice sheets – a chronological database and time-slice reconstruction, DATED-1.
615 *Boreas*, 45(1), 1–45. https://doi.org/10.1111/bor.12142
616
617 Ipsen, H.A., Principato, S.M., Grube, R.E., Lee, J.F. (2018). Spatial analysis of cirques from
618 three regions of Iceland: implications for cirque formation and palaeoclimate. *Boreas*
619 47, 565–576.

620 Kern, Z., & László, P. (2010). Size specific steady-state accumulation-area ratio: An
621 improvement for equilibrium-line estimation of small palaeoglaciers. *Quaternary Science*
622 *Reviews*, *29*(19–20), 2781–2787. https://doi.org/10.1016/j.quascirev.2010.06.033

623 Kleman, J., Stroeven, A.P. & Lundqvist, J. (2008). Patterns of Quaternary ice sheet erosion and
624 deposition in Fennoscandia and a theoretical framework for explanation. *Geomorphology*, 97(1-
625 2), 73–90. https://doi.org/10.1016/j.geomorph.2007.02.049
626
627 Křížek, M., & Mida, P. (2013). The influence of aspect and altitude on the size, shape and spatial
628 distribution of glacial cirques in the High Tatras (Slovakia, Poland). *Geomorphology*, 198, 57–
629 68. https://doi.org/10.1016/j.geomorph.2013.05.012

630 Lambeck, K., Smither, C., & Ekman, M. (1998a). Tests of glacial rebound models for
631 Fennoscandinavia based on instrumented sea- and lake-level records. *Geophysical Journal*
632 *International*, *135*(2), 375–387. https://doi.org/10.1046/j.1365-246X.1998.00643.x

633 Lambeck, K., Smither, C., & Johnston, P. (1998b). Sea-level change, glacial rebound and mantle
634 viscosity for northern Europe. *Geophysical Journal International*, 134(1), 102–144.
635 https://doi.org/10.1046/j.1365-246X.1998.00541.x

636 Lidmar-Bergström, K., Ollier, C. D., & Sulebak, J. R. (2000). Landforms and uplift history of
637 southern Norway. *Global and Planetary Change*, 24(3–4), 211–231.
638 https://doi.org/10.1016/S0921-8181(00)00009-6

639 Mangerud, J. (2008). The Early and Middle Weichselian in Norway: a review. *Boreas*, 10(4),
640 381–393. https://doi.org/10.1111/j.1502-3885.1981.tb00500.x

Mangerud, J., Gyllencreutz, R., Lohne, Ø., Svendsen, J. I. (2011). Glacial History of Norway. *Development of Quaternary Science*. Vol 15, 279–298. ISSN: 1571-0866. https://doi.org/10.1016/B978-0-444-53447-7.00022-2

Meierding, T. C. (1982). Late Pleistocene glacial equilibrium-line altitudes in the Colorado Front Range: A comparison of methods. *Quaternary Research*, *18*(3), 289–310. https://doi.org/10.1016/0033-5894(82)90076-X

Mitchell, S. G., & Humphries, E. E. (2014). Glacial cirques and the relationship between equilibrium line altitudes and mountain range height. *Geology*, *43*(1). https://doi.org/10.1130/G36180.1

Morris, S. E. (1981). Topoclimatic Factors and the Development of Rock Glacier Facies. *Arcticand Alpine Research*, *13*(3), 329–338. https://doi.org/10.1080/00040851.1981.12004253

Nielsen, S. B., Gallagher, K., Leighton, C., Balling, N., Svenningsen, L., Jacobsen, B. H., Thomsen, E., Nielsen O. B., Heilmann-Clausen, C., Egholm, D. L., Summerfield, M.A., Clausen, O.R., Piotrowski, J.A., Thorsen, M.R., Huuse, M., Abrahamsen, N., King, C., Lykke-Andersen, H. (2009). The evolution of western Scandinavian topography: A review of Neogene uplift versus the ICE (isostasy-climate-erosion) hypothesis. *Journal of Geodynamics*, *47*(2–3), 72–95. https://doi.org/10.1016/j.jog.2008.09.001

Nesje, A. (1992). Topographical effects on the equilibrium line altitude on glaciers. *GeoJournal* 27, 383–391.

Nesje, A. (2009). Latest Pleistocene and Holocene alpine glacier fluctuations in Scandinavia. *Quaternary Science Reviews*, 28(21–22), 2119–2136. https://doi.org/10.1016/j.quascirev.2008.12.016

Nesje, A., Bakke, J., Dahl, S. O., Lie, Ø., & Matthews, J. A. (2008). Norwegian mountain glaciers in the past, present and future. *Global and Planetary Change*, 60(1–2), 10–27. https://doi.org/10.1016/j.gloplacha.2006.08.004

Norwegian Meteorological Institute. (2021). Climate Norms. Retrieved April 23, 2021, from Norwegian Centre for Climate Services website: https://klimaservicesenter.no/kss/vrdata/normaler

Norwegian Mapping Authority (2016). The Terrain Model WMS Service Provides Information on the Terrestrial Terrain Model (DTM 10). https://www.kartverket.no/data/ Laserskanning/.

NVE. Norwegian Water Resources and Energy Directorate (NVE). Climate Indicator Products, http://glacier.nve.no/viewer/CI/, downloaded b2017.12.01N. (2017).

Ohmura, At.; Kasser, P., & Funk, M. (1992). Climate at the equilibrium line of glaciers. *Journal of Glaciology*, 38(130), 397–411. https://doi.org/10.3189/S0022143000002276

677 Ohmura, A., & Boettcher, M. (2018). Climate on the equilibrium line altitudes of glaciers:
678 Theoretical background behind Ahlmann's P/T diagram. *Journal of Glaciology*, 64(245), 489–
679 505. https://doi.org/10.1017/jog.2018.41

680 Oien, R. P., Spagnolo, M., Rea, B. R., Barr, I. D., & Bingham, R. G. (2020). Climatic controls on
681 the equilibrium-line altitudes of Scandinavian cirque glaciers. *Geomorphology*, 352.
682 https://doi.org/10.1016/j.geomorph.2019.106986

683 Olsen, L., Sveian, H., & Bergstrom, B. (2001). Rapid adjustments of the western part of the
684 Scandinavian ice sheet during the Mid- and Late Weichselian a new model. *Norsk Geografisk*
685 *Tidsskrift - Norwegian Journal of Geography*, 81(93–118).

686 Olsen, L., Sveian, H., Bergstrøm, B., Ottesen, D., & Rise, L. (2013a). Quaternary glaciations and
687 their variations in Norway and on the Norwegian continental shelf. *Quaternary Geology of*
688 *Norway, Geological Survey of Norway Special Publication*, 13, pp. 27–78.

689 Olsen, L., Sveian, H., Ottesen, D., & Rise, L. (2013b). Quaternary glacial, interglacial and
690 interstadial deposits of Norway and adjacent onshore and offshore areas. *Quaternary Geology of*
691 *Norway, Geological Survey of Norway Special Publication*, 13, pp. 79-144.

692 Olyphant, G. A. (1977). Topoclimate and the Depth of Cirque Erosion. *Geografiska Annaler,*
693 *Series A: Physical Geography*, 59(3), 209–213. Retrieved from
694 https://www.jstor.org/stable/520800

695 Pawlewicz, M.J., Steinshouer, D.W., Gautier, D.L. (2002), Map showing geology, oil and gas
696 fields, and geologic provinces of Europe including Turkey: U.S. Geological Survey Open-File
697 Report 97-470-I, 14 p., https://doi.org/10.3133/ofr97470I. ISSN: 2331-1258

698 Pearce, D. M., Ely, J. C., Barr, I. D., & Boston, C. M. (2017). Section 3.4.9: Glacier
699 Reconstruction. In *Geomorphological Techniques (Online Edition)* (Vol. 9). British Society for
700 Geomorphology.

701 Pedersen, V. K., Knutsen, Å. R., Pallisgaard-Olesen, G., Andersen, J. L., Moucha, R., &
702 Huismans, R. S. (2021). Widespread glacial erosion on the Scandinavian passive margin.
703 *Geology*, 49(8), 1004-1008. https://doi.org/10.1130/g48836.1

704 Peterson, J. A., & Robinson, G. (1969). Trend surface mapping of cirque floor levels. *Nature*,
705 Vol. 222, pp. 75–76. https://doi.org/10.1038/222075a0

706 Principato, S. M., & Lee, J. F. (2014). GIS analysis of cirques on Vestfirdir, northwest Iceland:
707 Implications for palaeoclimate. *Boreas*, *43*(4), 807–817. https://doi.org/10.1111/bor.12075

708 Rea, B. R., Pellitero, R., Spagnolo, M., Hughes, P., Ivy-Ochs, S., Renssen, H., Ribolini, A.,
709 Bakke, J., Lukas, S. and Braithwaite, R. J. (2020). Atmospheric circulation over Europe during
710 the Younger Dryas. *Science Advances*, *6*(50), eaba4844. https://doi.org/10.1126/sciadv.aba4844

Renssen, H., Isarin, R. F. B., Jacob, D., Podzun, R., & Vandenberghe, J. (2001). Simulation of the Younger Dryas climate in Europe using a regional climate model nested in an AGCM: preliminary results. *Global and Planetary Change*, *30*, 41–57.

Rosentau, A., Harff, J., Oja, T., & Meyer, M. (2012). Postglacial rebound and relative sea level changes in the Baltic Sea since the Litorina transgression. *Baltica*, *25*(2), 113–120. https://doi.org/10.5200/baltica.2012.25.11

Rudberg, S. (1994). Glacial cirques in Scandinavia. *Norsk Geografisk Tidsskrift - Norwegian Journal of Geography*, 48(4), 179–197. https://doi.org/10.1080/00291959408552343

Seppä, H., & Birks, H. J. B. (2001). July mean temperature and annual precipitation trends during the Holocene in the Fennoscandian tree-line area: pollen-based climate reconstructions. *The Holocene*, *11*(5), 527–539.

Spagnolo, M., Pellitero, R., Barr, I. D., Ely, J. C., Pellicer, X. M., & Rea, B. R. (2017). ACME, a GIS tool for Automated Cirque Metric Extraction. *Geomorphology*, 278, 280–286. https://doi.org/10.1016/j.geomorph.2016.11.018

Steer, P., Huismans, R. S., Valla, P. G., Gac, S., & Herman, F. (2012). Bimodal plio-quaternary glacial erosion of fjords and low-relief surfaces in Scandinavia. *Nature Geoscience*, *5*(9), 635–639. https://doi.org/10.1038/ngeo1549

Steffen, H., & Kaufmann, G. (2005). Glacial isostatic adjustment of Scandinavia and northwestern Europe and the radial viscosity structure of the Earth's mantle. *Geophysical Journal International*, *163*(2), 801–812. https://doi.org/10.1111/j.1365-246X.2005.02740.x

Stroeven, A.P., Hättestrand, C., Kleman, J., Heyman, J., Fabel, D., Fredin, O., Goodfellow, B.W., Harbor, J.M., Jansen, J.D., Olsen, L. Caffee, M.W., Fink, D., Lundqvist, J., Rosqvist, G.C., Strömberg, B. & Jansson, K. (2016). Deglaciation of fennoscandia. *Quaternary Science Reviews*, 147, 91–121. https://doi.org/10.1016/j.quascirev.2015.09.016

Sutherland, D. G. (1984). Modern glacier characteristics as a basis for inferring former climates with particular reference to the Loch Lomond Stadial. *Quaternary Science Reviews*, *3*(4), 291–309. https://doi.org/10.1016/0277-3791(84)90010-6

Torsnes, I., Rye, N., & Nesje, A. (1993). Arctic and Alpine Research Modern and Little Ice Age Equilibrium-line Altitudes on Outlet Valley Glaciers from Jostedalsbreen, Western Norway: An Evaluation of Different Approaches to their Calculation. *Arctic and Alpine Research*, 25(2), 106–116. https://doi.org/10.1080/00040851.1993.12002990

Tveito, O. E., Førland, E., Heino, R., Hansen-Bauer, I., Alexandersson, H., Dahlström, B., Drebs, A., Kern-Hansen, C., Jónsson, T., Laursen, E. V., & Westman, Y. (2000). DNMI - Nordic temperature maps. In *DNMI - Report: Vol. 09/00 KLIM*. Norwegian Meterological Institute.

746 Vilborg, L. (1977). The Cirque Forms of Swedish Lapland Author. *Geografiska Annaler, Series*
747 *A: Physical Geography*, *59*(3), 89–150. https://doi.org/https://www.jstor.org/stable/520796

748 Vilborg, L. (1984). The Cirque Forms of Central Sweden. *Geografiska Annaler, Series A:*
749 *Physical Geography*, *66*(1), 41–77. https://doi.org/https://www.jstor.org/stable/520939

750

751 Wallick, K. N., & Principato, S. M. (2020). Quantitative analyses of cirques on the Faroe
752 Islands: evidence for time transgressive glacier occupation. *Boreas*, *49*(4), 828–840.
753 https://doi.org/10.1111/bor.12458

754 Winkler, S., Elvehy, H., & Nesje, A. (2009). Glacier fluctuations of Jostedalsbreen, western
755 Norway, during the past 20 years: The sensitive response of maritime mountain glaciers. *The*
756 *Holocene*, *19*(3), 395–414. https://doi.org/10.1177/0959683608101390

757 Winsvold, S. H., Andreassen, L. M., & Kienholz, C. (2014). Glacier area and length changes in
758 Norway from repeat inventories. *The Cryosphere*, 8, 1885–1903. https://doi.org/10.5194/tc-8-
759 1885-2014